

In Situ Vertical Growth of Fe–Ni Layered Double-Hydroxide Arrays on Fe–Ni Alloy Foil: Interfacial Layer Enhanced Electrocatalyst with Small Overpotential for Oxygen Evolution Reaction

Qian Xiang,[†] Fan Li,[†] Wenlong Chen,[†] Yanling Ma,[†] Yi Wu,[†] Xin Gu,[†] Yong Qin,[†] Peng Tao,[†] Chengyi Song,[†] Wen Shang,[†] Hong Zhu,^{*,†,‡,§} Tao Deng,^{*,†,||} and Jianbo Wu^{*,†,§,||}

[†]State Key Laboratory of Metal Matrix Composites, School of Materials Science and Engineering, Shanghai Jiao Tong University, 800 Dongchuan Road, Shanghai, 200240, PR China

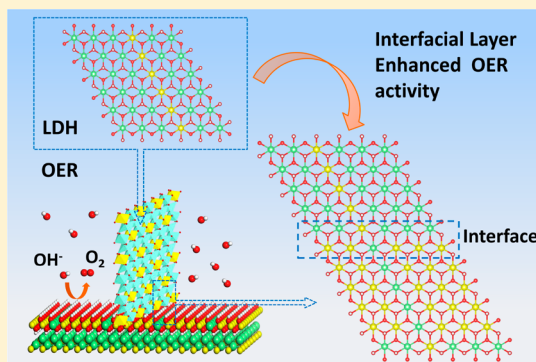
[‡]University of Michigan - Shanghai Jiao Tong University Joint Institute, Shanghai Jiao Tong University, Shanghai 200240, PR China

[§]Materials Genome Initiative Center, Shanghai Jiao Tong University, Shanghai 200240, PR China

^{||}Hydrogen Science Research Center, Shanghai Jiao Tong University, Shanghai 200240, PR China

Supporting Information

ABSTRACT: Layer double hydroxide (LDH) has been widely applied to electrocatalysis, especially toward the oxygen evolution reaction (OER), owing to its flexible layered structure and multifunctionality. Herein, FeNi LDH nanosheet arrays are directly synthesized on various metal foils by a facile hydrothermal method. Compared with single Fe or Ni substrates, the obtained FeNi LDH/FeNi foil exhibited an ultrasmall onset overpotential of ~90 mV, high catalytic activity (overpotential of 130 mV @ 10 mA/cm²), and durable stability in 0.1 M KOH electrolyte. We also demonstrate, by utilizing density functional theory calculations, that the growth of the hydroxide interfacial layer between LDH and FeNi foil makes the LDH possess more favorable adsorption to the OH intermediate during OER than the pure LDH. This reveals that the vertical FeNi LDH arrays on the FeNi alloy substrate are prone to be an efficient catalyst toward OER.



Electrochemical water splitting, which contains the anodic oxygen evolution reaction (OER) and cathodic hydrogen evolution reaction (HER), is attracting more and more attention as a promising technology to produce clean energy.^{1–3} Compared with HER, OER became the major challenge because of its sluggish kinetics and initiation at high potential (at least 1.23 V vs the reversible hydrogen electrode (RHE)).⁴ Therefore, it is essential to reduce the dynamic overpotential and improve the catalytic efficiency to identify active OER electrocatalysts.^{2,3} Currently, the most practical OER electrocatalysts are mainly noble metal-based IrO₂ and RuO₂. However, their widespread application is still a challenge constrained by the element scarcity and high cost.^{5,6} To this end, it is urgent to develop effective catalysts, earth-abundant metals, or inexpensive transition-metal-based

oxides^{7,8} or hydroxides^{9,10} that can be employed to catalyze OER.^{11–14}

Typically, ordered geometrically confined architectures with large surface area, uniform structure, and high porosity would have fascinating properties in electrocatalysis.^{15–19} Recently, LDH with a brucite-like layered crystal structure^{20–22} has been widely studied, owing to its increasingly broad applications in several fields, including catalysis and electrochemistry.^{20,23,24} It provides more active sites on the surface than traditional nanoparticles, which benefits from its macroporous nanosheet architecture.^{25–28}

Received: August 10, 2018

Accepted: September 10, 2018

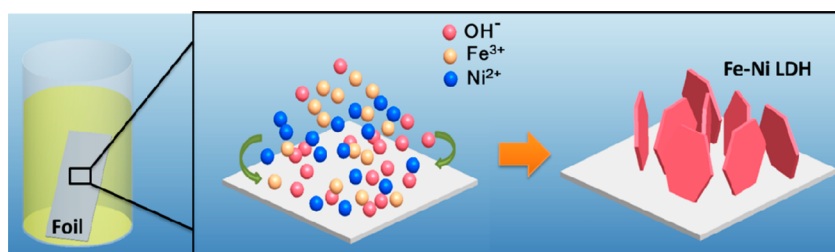


Figure 1. Schematic illustration for the process to synthesize FeNi LDH sheets on the Fe, Ni, and FeNi alloy foils with Fe and Ni salts.

For now, iron and nickel oxyhydroxide electrocatalysts with three-dimensional (3D) architecture were proved to be highly active catalysts in base media toward OER.^{29–38} The high surface area structure of FeNi LDH is usually synthesized by the hydrothermal method, and at the same time, the multiporous and interlayer architecture could provide more active sites for the intermediates. Lu et al.³⁸ prepared 3D FeNi LDH on Ni foam, which showed an overpotential of ~ 230 mV in 0.1 M KOH. However, the electrical conductivity of LDH is unsatisfactory; therefore, many kinds of substrates were investigated to further improve the OER performances of the FeNi LDH, such as carbon nanotubes (CNTs) and graphene.^{13,39–43} Most substrates are freestanding particles, which tend to undergo severe aggregation during the preparation of the electrode, leading to great loss of the active sites. Furthermore, such aggregated FeNi LDH leaves poor contact with the conductive substrate for every single nanosheet, simultaneously avoiding a large portion of the interlayer transfer of electrons, which causes a larger overpotential. There are few reports on the in situ vertically grown 2D FeNi LDH arrays on foils, which exhibit both high accessible active sites as well as good contact between 2D FeNi LDH and the substrate. Recently, Wang et al. synthesized FeNi LDH nanosheets on NiCo₂O₄ nanowires which presented a small overpotential of 290 mV in 1 M KOH.⁴⁴ However, most of the reported FeNi LDH still proceeds with large overpotential, and the mechanism of the improvement promoted by the substrate is still unanswered.

Herein, by adopting Fe, Ni, and bimetallic FeNi alloy foils as the substrates, FeNi LDH nanosheet arrays with a large number of active sites and enhanced electron conductivity between catalysts and the substrates were obtained. It is worth noting that the FeNi LDH on FeNi alloy foil showed outstanding OER activities with a largely reduced onset overpotential (the onset overpotential is determined by the tangent method; see the details in the Supporting Information) of ca. 1.32 V vs RHE, namely, an onset overpotential of 90 mV and long-term durability in the alkaline electrolyte of 0.1 M KOH, indicating excellent performance as a promising catalyst toward OER.

FeNi LDH nanosheets grown vertically on various metal foils (Fe, Ni, and FeNi alloy) can be achieved via a facile hydrothermal method by directly immersing the substrates into the corresponding reaction solutions, as illustrated in Figure 1. Briefly, the preparation of FeNi LDH nanosheets involved precipitation of iron and nickel nitrates on metal foil in aqueous solution, which is induced by urea hydrolysis in an alkaline solution upon hydrothermal treatment at 120 °C for 12 h (see the details in the Experimental Section in the Supporting Information). Because FeNi LDH is a typical LDH, ions and molecules can be present between the stacking layers along the *c*-axis.⁴⁵ During the reaction process, urea

decomposed into ammonia and carbonate, which served as the intercalated anion.³⁸ CO₃²⁻ generated by the decomposition of the urea is inclined to adsorb on the (001) surface, passivating this plane. As a result, the growth of planes along the [001] direction is suppressed.^{46,47} Therefore, the FeNi LDH crystals are stacked in the direction vertical to the substrate surface.

The vertical 2D FeNi LDH nanosheet arrays on different metal foils are shown in Figure 2. After the reaction, the pale brown films could be observed on the surface of three substrates (Figure S1). Apparently, the well-defined hexagonal-like nanosheets grew vertically on each foil directly, forming a uniform and porous FeNi LDH layer (Figure 2a–c). The morphologies of the grown FeNi LDH on different substrates were similar, while the sizes showed a slight difference between them. The FeNi hydroxide hexagonal sheets on different foils had a thickness of approximately 15–25 nm and sizes ranging from about 400 to 650 nm (Figures S2 and S3). XRD patterns of the substrates and FeNi LDH on foils (Figures 2d and S4) showed strong diffraction peaks of the substrates, and the broad diffraction peaks at the region of 15° and 22° indicated the hydroxide of Ni and Fe, which matched well with the typical pattern of LDH materials reported in previous work.^{38,48} The HAADF-STEM image and STEM-EDX elemental images of the FeNi LDH sheets on foils (Figure 2e–g) showed that the Fe, Ni, and O elements were uniformly distributed on the LDH architectures, which demonstrated the formation of the hydroxides of iron and nickel.

In order to exclude the influence of the different substrates, the bonding states of Fe, Ni, and O were further analyzed by XPS (Figures 3 and S5). The binding energy peaks of Fe 2p_{3/2} were located at 709.8 eV (on FeNi foil), 712.2 eV (on Fe foil), and 711.8 eV (on Ni foil) (Figure 3d–), indicating the existence of Fe³⁺.³² The Ni 2p_{3/2} peaks located at 855.6 eV (on FeNi foil), 856.7 eV (on Fe foil), and 855.3 eV (on Ni foil) indicated the existence of Ni²⁺ oxidation states (Figure 3g–i).³²

Herein, the OER performances of the as-prepared FeNi LDH on different foils were evaluated in a conventional three-electrochemical setup in O₂-saturated 0.1 M KOH electrolyte at 25 °C. The i-R corrected CV curve of FeNi LDH on FeNi foil (Figure 4a) revealed the redox couple from Ni(II) to Ni(III) at 1.25 V vs RHE.³⁸ The positive (oxidation) current at potentials greater than 1.35 V vs RHE was ascribed to OER. The redox couple in the LDH on Fe and Ni foils occurred at a higher potential than the FeNi LDH sheet/FeNi. The FeNi LDH sheet/FeNi exhibited excellent OER performance compared with the FeNi LDH sheets on the other two substrates (Figures 4a and S6a). The FeNi LDH sheet/FeNi showed the lowest reported onset overpotential of 90 mV and the smallest overpotential of 130 mV at 10 mA/cm² in 0.1 M KOH to date (Tables S1 and S2), which were much lower than

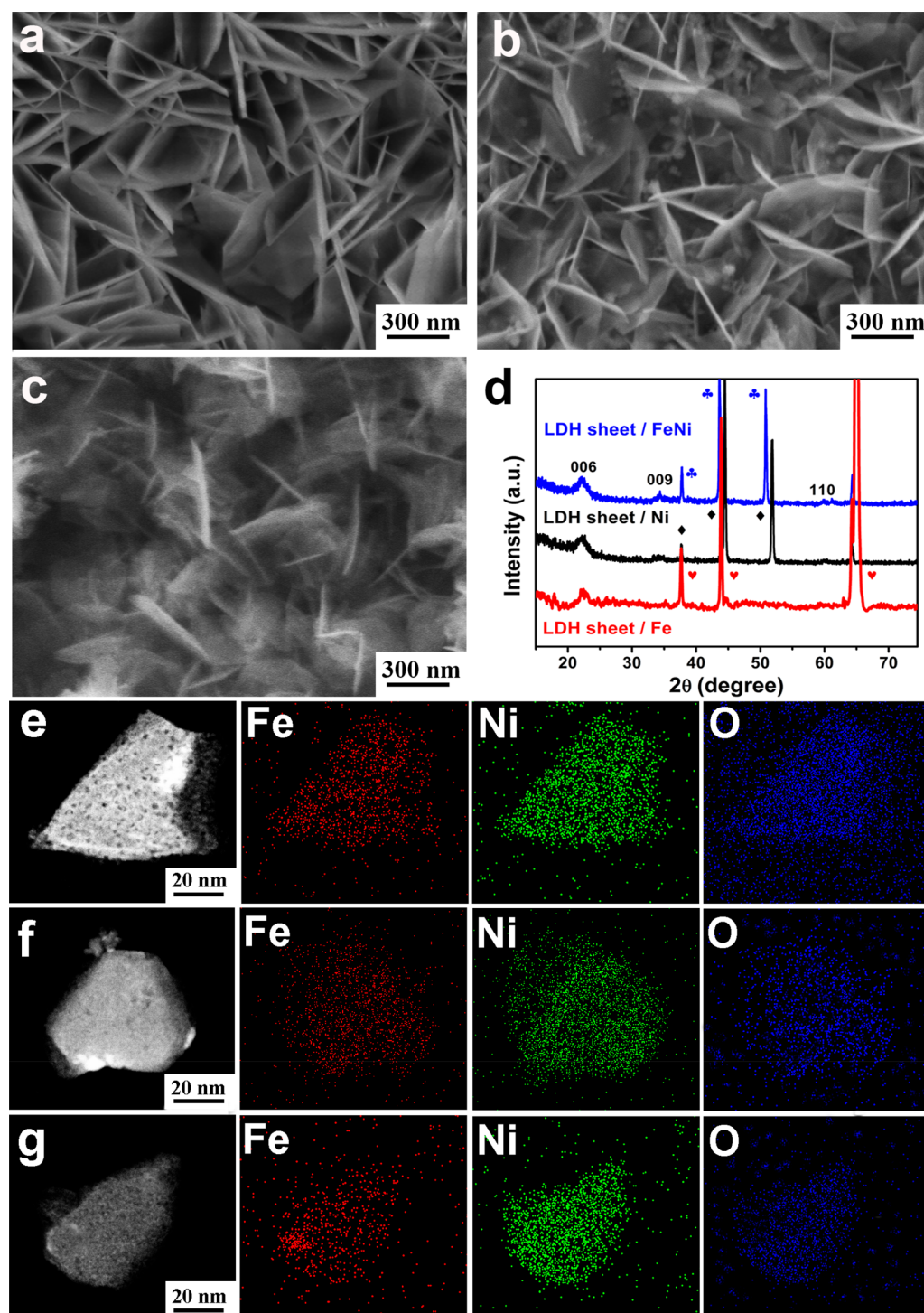


Figure 2. SEM characterization of the catalyst electrodes FeNi LDH sheets on (a) FeNi alloy foil, (b) Fe foil, and (c) Ni foil. (d) XRD patterns of FeNi LDH on Fe, Ni, and FeNi foils. HAADF-STEM image and STEM-EDX elemental maps of FeNi LDH sheets on (e) FeNi foil, (f) Fe foil, and (g) Ni foil.

that of the FeNi LDH sheet/Fe, FeNi LDH sheet/Ni, and IrO₂ (Figure S7). The overpotentials of them were 210 mV/390 mV, 220 mV/410 mV (inset of Figure 4a and magnification image in Figure S8), and 270 mV/390 mV, respectively. The loading amounts of the catalysts on foils were shown in Table S2. The loading mass of the FeNi LDH sheet/FeNi was 0.1 mg/cm², which showed better activity with less loading than those of the LDH on Fe (0.15 mg/cm²), Ni foils (0.1 mg/cm²), and the commercial IrO₂ (0.2 mg/cm²). It is notable that

the bare FeNi alloy foil exhibited an onset potential of 1.43 V vs RHE (Figure S6b). The activity was also normalized based on the intrinsic metrics, including both mass activity (A/g) and turnover frequency (TOF)⁴⁹ in Figure 4 and Table S3. The FeNi LDH sheet/FeNi showed excellent performance of 101 A/g at 130 mV and 538 A/g at 250 mV compared to that of the other two electrodes (Figure 4b). A total-metal TOF (TOF_m), which is essentially an average TOF for all the metals in LDH sheets, was measured according to the previous

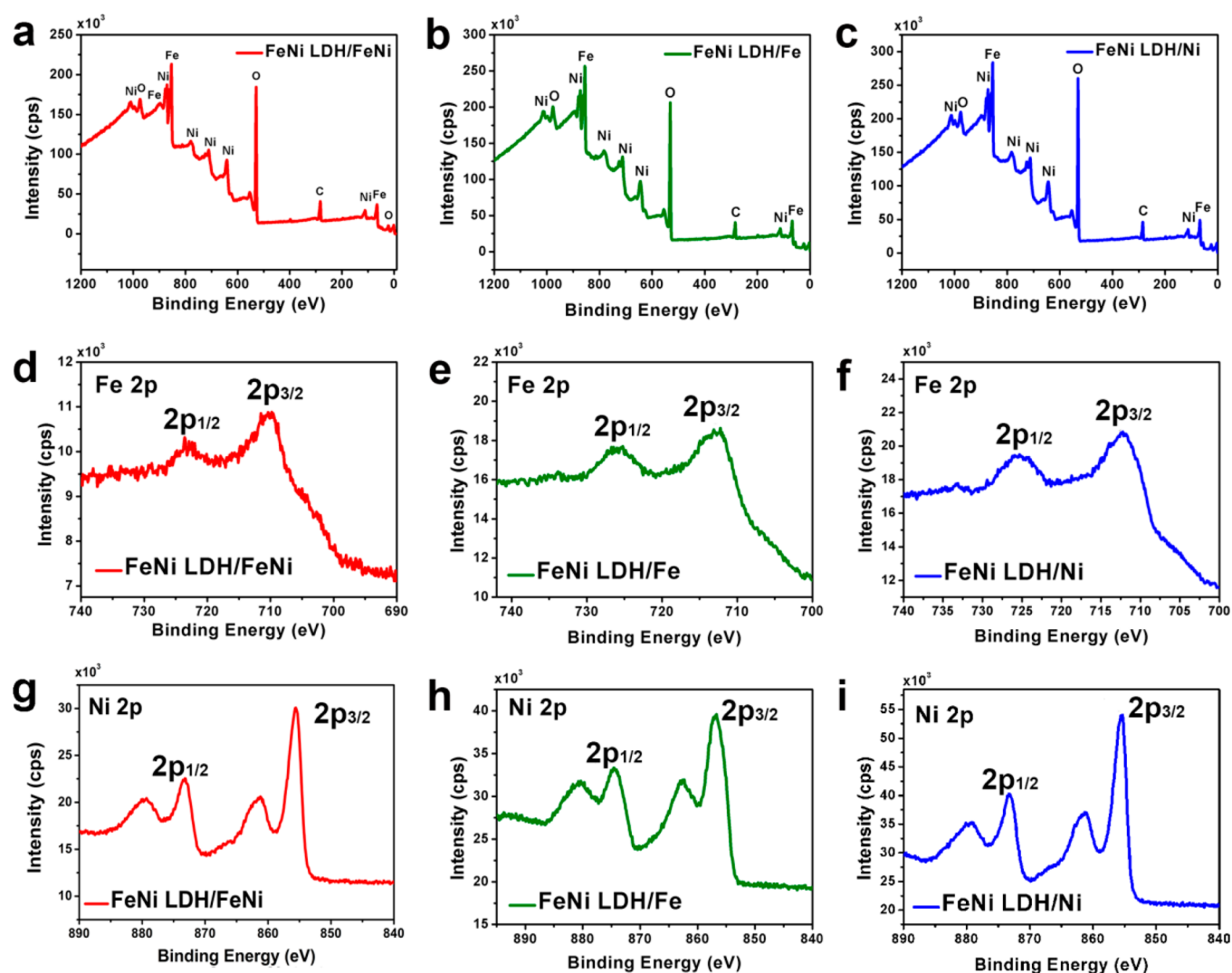


Figure 3. XPS spectra of the FeNi LDH sheets on foils. (a–c) Full-scan XPS spectra. High-resolution XPS spectra of (d–f) Fe element and (g–i) Ni element.

reported method.⁴⁹ The total number of metal sites was obtained from the inductively coupled plasma optical (ICP) measurement (Table S4). The TOF_{tm} values of FeNi LDH on different foils at 250 mV were 0.072 s⁻¹ (FeNi foil), 0.0036 s⁻¹ (Fe foil), and 0.0016 s⁻¹ (Ni foil) (Figure 4c and Table S3). Figure 4d displays the Tafel plots of FeNi LDH catalysts which were derived from the *i*-R corrected polarization curves with the scan rate of 1 mV/s (Figure S6) to gain more insight into OER activity of the FeNi LDH on different foils. The FeNi LDH sheet/FeNi foil performed the lowest Tafel slope of 39.8 mV·dec⁻¹ compared with those on Fe foil (54.8 mV·dec⁻¹) and Ni foil (57.6 mV·dec⁻¹), which further indicated its highest OER activity among the three samples.⁵⁰ Nyquist plots results (Figures 4e and S9) demonstrated that all these catalysts possessed small charge-transfer resistance, among which the bare FeNi alloy foil indeed showed the smallest resistance, indicating the fastest electron-transfer process on this FeNi alloy substrate (Table S5).⁵¹

The double-layer capacitances, C_{dl} , for the three electrodes were determined by the cyclic voltammetry (CV) measurements performed at various scan rates (Figure S10). The calculated value of double-layer capacitance for FeNi LDH/FeNi was 1665 $\mu\text{F}/\text{cm}^2$, which was much higher than that of

FeNi LDH/Fe (79.2 $\mu\text{F}/\text{cm}^2$) and FeNi LDH/Ni (200 $\mu\text{F}/\text{cm}^2$). Because the C_{dl} is proportional to the surface area and the conductivity of the materials, more active sites on FeNi LDH/FeNi are also responsible for excellent OER activity.^{46,52}

In this case, the double-layer capacitances of the bare foils were also performed in Figure S11. The bare FeNi foil showed double-layer capacitance (732.4 $\mu\text{F}/\text{cm}^2$) that was much higher than that of the other bare electrodes (Ni foil, 109.8 $\mu\text{F}/\text{cm}^2$; Fe foil, 52.8 $\mu\text{F}/\text{cm}^2$), which demonstrated that the FeNi substrate made an indispensable contribution to the excellent capacitance properties of FeNi LDH/FeNi catalyst. Furthermore, in order to analyze the OH diffusion coefficient (D_{OH}), CV curves of all the samples at various scan rates are displayed in Figure S12a–c. The D_{OH} of the electrode could be evaluated from the slope of the plots referred to the Sevcik equation⁵³ (see the analytical details in the Supporting Information). It is noteworthy the slopes (K) of the cathodic peak current (J_p) versus $\nu^{1/2}$ are in the order $K_{\text{FeNi}} > K_{\text{Fe}} > K_{\text{Ni}}$ (Figure S12d). Therefore, the order of the D_{OH} of the samples from the highest to the lowest is $D_{\text{FeNi}} > D_{\text{Fe}} > D_{\text{Ni}}$. The increase of D_{OH} means that the sample has a short ion diffusion path. It also indicates that the active sites in FeNi LDH have many more opportunities to interact with the electrolyte

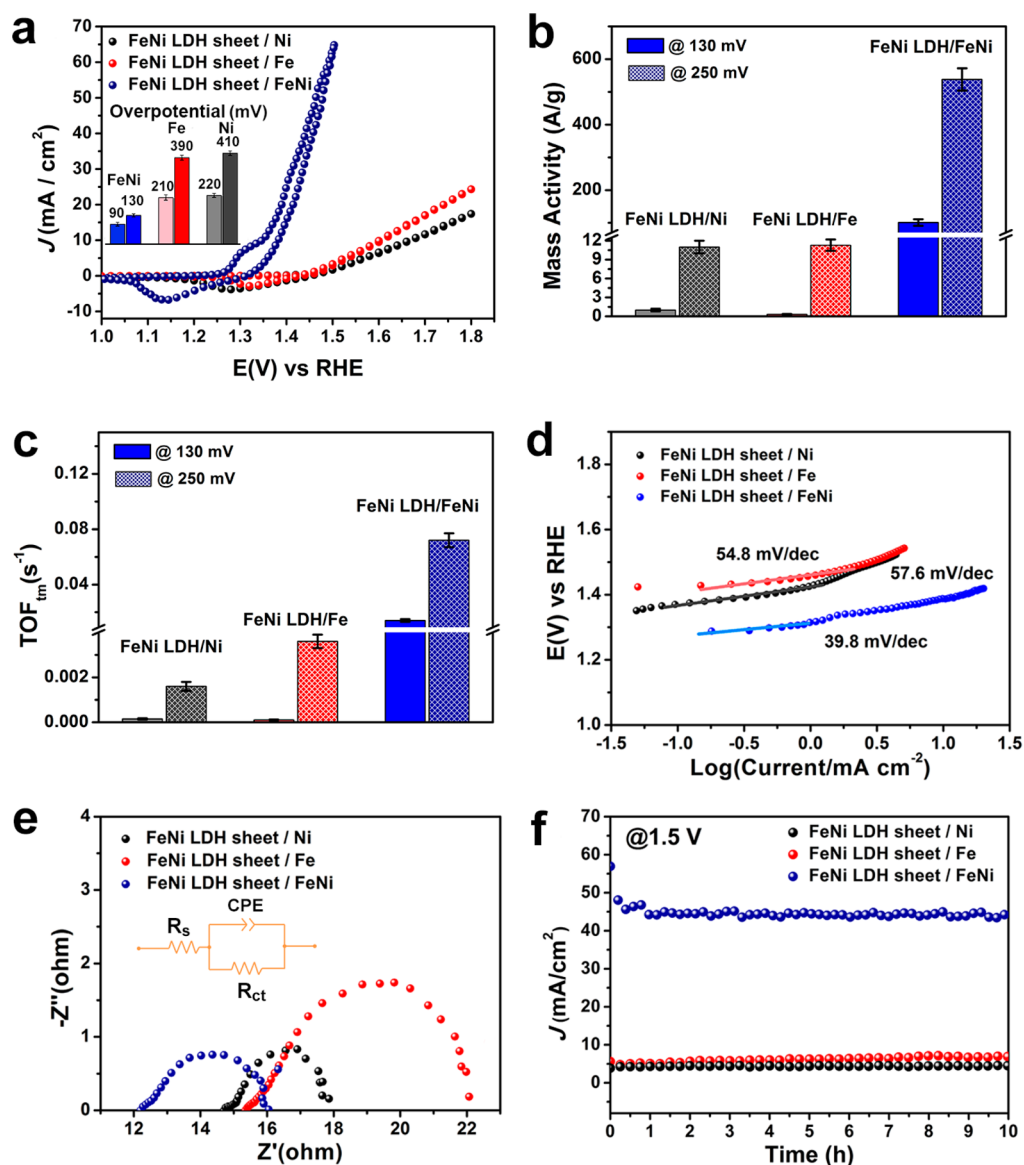


Figure 4. OER activities of the different catalysts. (a) CV curves of FeNi LDH for OER on different substrates as Ni, Fe, and FeNi alloy foils. The insert histogram in panel a shows the onset overpotentials and overpotentials at 10 mA/cm^2 of FeNi LDH sheets. Note: the CV curves have been i-R corrected. (b) Mass activity (A/g) for the FeNi LDH on foils at the specific overpotential. (c) Turnover frequency (TOF_{tm}) of the FeNi LDH on foils at the specific overpotential. (d) Tafel plots of FeNi LDH on different substrates as Ni, Fe, and FeNi alloy foils. (e) Nyquist plots of FeNi LDH on foils. The inset equivalent circuit consists of a resistance (R_s) (electrical conductivity), a charge-transfer resistance (R_{ct}) (interfacial electrocatalytic reaction between electrode and electrolyte), and a constant phase element (CPE). (f) Chronoamperometry experiments of the FeNi LDH on foils at 1.5 V vs RHE for 10 h.

solution, which in turn will favor faster ionic OH transportation, accelerating the electrode reaction during the OER process.^{53–55} In conclusion, the obtained D_{OH} of FeNi LDH/FeNi was the highest compared with those on Fe and Ni substrates, which also contributed to the excellent OER performance. The durability measurements of the FeNi LDH sheets on different foils proved that all of these FeNi LDH sheets on FeNi, Fe, and Ni foils had good stability; even so, the LDH on FeNi foil showed higher current density than those on Fe or Ni foil (Figure 4f). TEM images (Figure S13a–c) of the FeNi LDH sheets on different foils after stability testing were in a good accordance with the observation of FeNi LDH sheets before the measurements. The XRD pattern results (Figure S13d–f) after the testing also indicated the same peaks of the materials as the patterns before the stability test. The SEM

characterization revealed that the surface structure of FeNi LDH/FeNi was essentially retained after OER stability testing for 10 h (Figure S14a,b), while the 3D structure of nanosheet arrays on Fe and Ni foils were destroyed and collapsed after the stability test observed from Figure S14c–f, suggesting the outstanding morphology stability of FeNi LDH sheets on FeNi foil in OER.

Compared with the FeNi LDH on Fe foil and Ni foil (Figure 4a), the OER performance of LDH on FeNi substrate was increased sharply with an extremely small onset potential of 1.32 V vs RHE. The bare FeNi foil has an onset potential of 1.43 V vs RHE (Figure S6) with an overpotential of 200 mV, which is smaller than that of Fe (420 mV) or Ni (400 mV) foils because of its excellent conductivity and synergistic effect of the alloy elements of Fe and Ni,^{56,57} which also enhanced

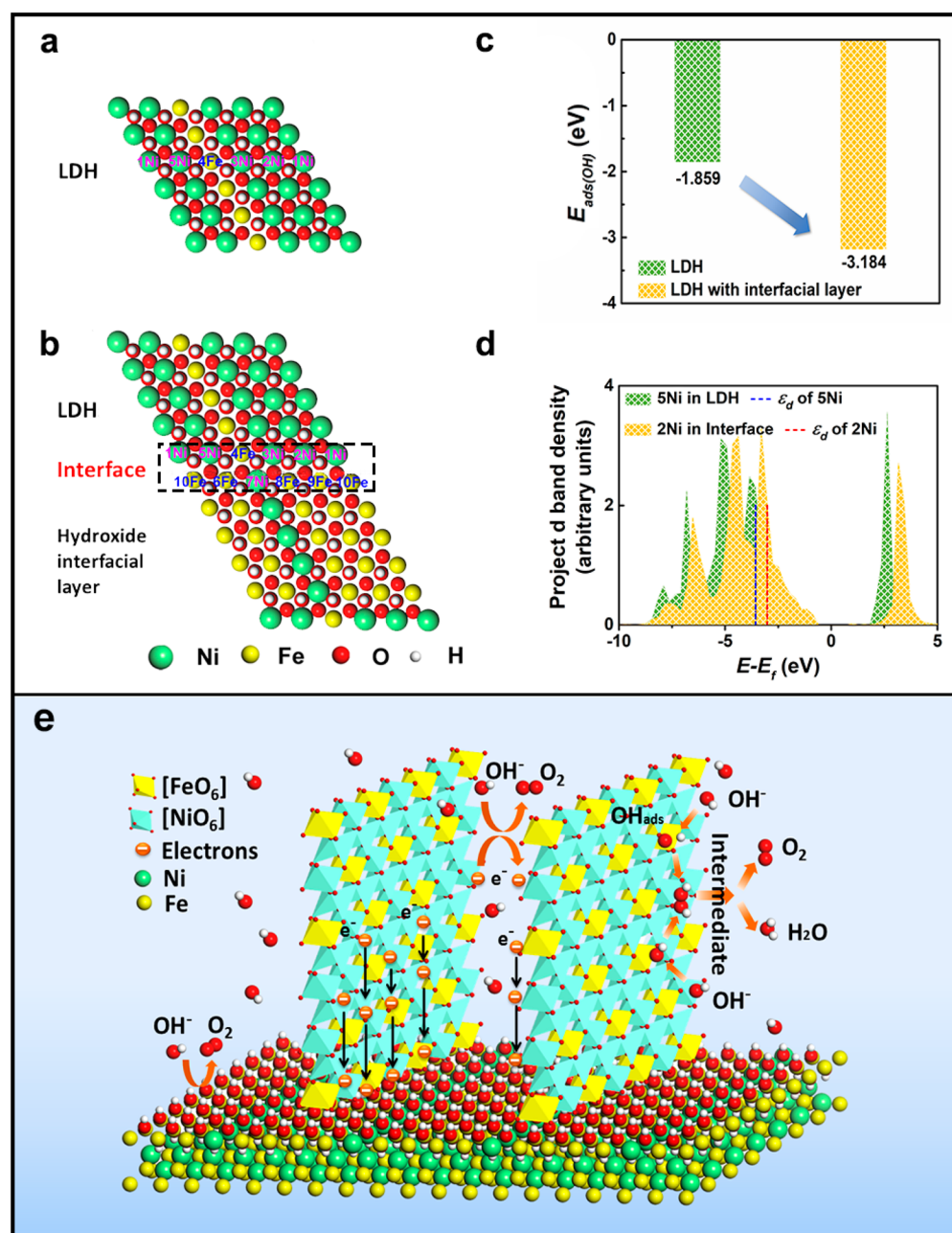


Figure 5. Adsorption sites of OH on (a) FeNi LDH and (b) FeNi LDH with hydroxide interfacial layer. (c) Comparison of adsorption energies for OH on FeNi LDH and FeNi LDH with hydroxide interfacial layer. (d) Comparison of d band center (ϵ_d) and d band density of Ni atom from stable adsorption site in FeNi LDH and FeNi LDH with hydroxide interfacial layer slabs. Note: $E-E_f$ indicates energy referenced Fermi level. (e) Schematic illustration of the OER process on FeNi LDH with hydroxide interfacial layer supported on FeNi alloy foil.

the OER performance after the in situ growth of the FeNi LDH. In addition, we found that a FeNi hydroxide interfacial layer was generated on the FeNi alloy foil during the growth of LDH on the FeNi foil (Figure S15). After scraping off the FeNi LDH sheets, the XRD pattern of the interfacial hydroxide layer on FeNi foil (Figure S16) revealed that its corresponding crystal phase was almost similar to the FeNi LDH sheets (Figure 2d), which matched well with the typical pattern (PDF 51-0463) of FeNi LDH materials reported in previous works.⁴⁸ The element composition of the FeNi LDH identified by XPS was 4:1 (Ni:Fe), while the ratio of the FeNi hydroxide interfacial layer on the FeNi foil was 1:3 (Ni:Fe) (Table S6). To sum up, the FeNi LDH sheets and the interfacial hydroxide

layer on FeNi foil have the same crystal structure but different compositions. Therefore, the excellent OER performance of the FeNi LDH on FeNi substrate can be attributed to the zero misfit between the FeNi hydroxide interfacial layer and LDH sheets with good cooperativity, which helps to increase the electron transfer at the interface between the self-supported catalysts layer and the supporting electrode.

For comparison, we further characterized the interlayers on the Ni and Fe foils (Figures S17–S20). The SEM analysis showed the interlayer on the Ni foil, and no crystalline structures were found (Figure S17a). The EDX results (Figure S17b–e) showed that Ni distributed uniformly on the Ni foil, corresponding to the XRD patterns of Ni, which show only the

Ni phase but no Ni hydroxide (Figure S18). On the Fe foil, the Fe and O elements dispersed uniformly on the surface (Figure S19), consistent with the formation of FeOOH based on the XRD analysis (Figure S20).^{58,59} These results indicated that it is difficult to form the FeNi hydroxide interfacial layer on both Ni and Fe foils.

To reveal the effect of the FeNi hydroxide interfacial layer between FeNi LDH and FeNi alloy foil on the enhanced OER performance, DFT calculations were carried out on the base of the FeNi LDH model (Figure 5a) and the FeNi LDH with hydroxide interfacial layer model (Figure 5b). The calculated adsorption energy of OH on the stable adsorption site among various possible adsorption sites (Figure 5a,b) revealed that OH was prone to adsorb on the surface of FeNi LDH with hydroxide interfacial layer with a OH adsorption energy of -3.184 eV, which is lower than the OH adsorption energy on the pure FeNi LDH (-1.859 eV), as displayed in Figure 5c. We further calculated the number of atomic charge differences (Δq) of surface metal atoms before and after OH adsorption on the surface of the pure FeNi LDH and FeNi LDH with hydroxide interfacial layer, respectively, using Bader charge analysis,⁶⁰ as shown in Tables S9 and S10. The changes of charge populations for surface metal atoms upon OH adsorption are larger in FeNi LDH with hydroxide interfacial layer compared to that for the pure FeNi LDH. To further investigate the interfacial interactions, the d band centers (ε_d) and projected d band densities (Figure 5d) of Ni atom from the stable adsorption site in the pure FeNi LDH and FeNi LDH with hydroxide interfacial layer slabs were determined, respectively. Figure 5d showed that the ε_d of Ni in the pure FeNi LDH was lower than ε_d of Ni in FeNi LDH with hydroxide interfacial layer slabs. The relatively upper position of the ε_d toward Ni in FeNi LDH with hydroxide interfacial layer slabs gives rise to the increasing number of empty antibonding state and then a stronger bond between adsorbate and surface.⁶¹ Therefore, OH has a stronger tendency to adsorb on the surface of FeNi LDH with hydroxide interfacial layer than the pure FeNi LDH because of the interfacial interaction mainly including the modification effect of electron transfer and d band center shifting. Considering that the first release of a proton from an adsorbed water molecule, leaving an adsorbed OH, was the rate-determining step of the OER process,^{12,62,63} the Gibbs free energies of the corresponding intermediates decreased efficiently because of the increased OH adsorption, facilitating the dissociation of the O–H bond of the H₂O. Accordingly, the synergistically enhanced interplay between FeNi LDH and hydroxide interfacial layer produced a favorable local coordination environment and electronic structure to adsorb OH intermediates, eventually promoting the OER process.⁵⁴

The schematics showed that OH⁻ from the electrolyte adsorbed on the active catalyst site on the LDH and then reacted with other dissociative OH⁻ to form a reaction intermediate (recombination), which is then further oxidized to O₂ (Figure 5e). In FeNi LDH sheet structures, the increased charge of Fe³⁺ relative to Ni²⁺ requires the compensation of additional anions like OH⁻ between the sheets, which causes the larger intersheet spacing compared to the hydroxide of single metal like Ni(OH)₂.^{64,65} Consequently, the increased intersheet spacing would facilitate the transport of OH⁻/O₂ through the layer.⁶⁶ Therefore, these vertically grown FeNi LDH nanosheet arrays not only create many nanoscale channels for the reaction intermediates to access the most

active sites on the surface of 2D sheets but also ensure the direct contact of each individual 2D sheet with the FeNi substrate and largely promote the intralayer electron transfer, both of which avoid the interlayer electron transfer and therefore dramatically improve the electron transfer as well as the catalytic activity.^{25–28} Furthermore, the synergistic effect between FeNi LDH and the FeNi hydroxide layer modified a favorable local chemical environment and a proper electronic structure to adsorb OH intermediates for boosting the OER process.

In summary, the well-defined FeNi LDH nanosheet arrays with microporous architecture are grown vertically in situ on the Fe, Ni, and FeNi alloy foils, respectively. The obtained FeNi LDH 2D sheet arrays on FeNi alloy foil exhibited an onset overpotential of 90 mV with enhanced catalytic activity (130 mV at 10 mA/cm²) (Figure S21) and stable durability in alkaline 0.1 M KOH electrolyte. This unprecedented small onset overpotential of 90 mV is mainly due to the following three points: (1) The in situ vertically grown 2D sheets architecture optimizes the access of active sites for OER. (2) The contact between the side surface of FeNi LDH sheets and the substrate improves the intralayer electron and ion transfer with the highest OH diffusion coefficient (D_{OH}). (3) DFT calculation proves that the synergistic enhanced interaction between FeNi LDH and the interfacial hydroxide layer produces a more inclination to adsorb OH and the OER intermediates, eventually promoting the OER process. The FeNi LDH arrays on FeNi foil and the bare FeNi foil both had small onset potential (1.32 V vs RHE and 1.43 V vs RHE), indicating that the FeNi alloy substrate was desirable for FeNi LDH-based OER catalysts, which should be widely studied in the future.

■ ASSOCIATED CONTENT

📄 Supporting Information

The Supporting Information is available free of charge on the ACS Publications website at DOI: 10.1021/acseenergylett.8b01466.

Experimental Section; Figures S1–S21 and Tables S1–S10 as described in the text (PDF)

■ AUTHOR INFORMATION

Corresponding Authors

*E-mail: jianbowu@sjtu.edu.cn.

*E-mail: dengtao@sjtu.edu.cn.

*E-mail: hong.zhu@sjtu.edu.cn.

ORCID

Peng Tao: 0000-0002-9284-7158

Chengyi Song: 0000-0002-4757-9481

Wen Shang: 0000-0002-6984-3060

Hong Zhu: 0000-0001-7919-5661

Tao Deng: 0000-0002-1560-3838

Jianbo Wu: 0000-0002-3574-5585

Notes

The authors declare no competing financial interest.

■ ACKNOWLEDGMENTS

The work is sponsored by the thousand talents program for distinguished young scholars from the Chinese government, National Key R&D Program of China (No. 2017YFB0406000), the National Science Foundation of

China (21875137, 51521004, and 51420105009), and start-up fund (J.W.) and the Zhi-Yuan Endowed fund (T.D.) from Shanghai Jiao Tong University. H.Z. acknowledges the financial support from the Shanghai Sailing Program (16YF1406000) and the computing resources from Shanghai Jiao Tong University Supercomputer Center.

REFERENCES

- (1) Mallouk, T. E. Water Electrolysis: Divide and Conquer. *Nat. Chem.* **2013**, *5*, 362–363.
- (2) Li, X.; Hao, X.; Abudula, A.; Guan, G. Nanostructured Catalysts for Electrochemical Water Splitting: Current State and Prospects. *J. Mater. Chem. A* **2016**, *4*, 11973–12000.
- (3) Wang, J.; Cui, W.; Liu, Q.; Xing, Z.; Asiri, A. M.; Sun, X. Recent Progress in Cobalt-Based Heterogeneous Catalysts for Electrochemical Water Splitting. *Adv. Mater.* **2016**, *28*, 215–230.
- (4) Luo, J.; Im, J. H.; Mayer, M. T.; Schreier, M.; Nazeeruddin, M. K.; Park, N. G.; Tilley, S. D.; Fan, H. J.; Grätzel, M. Water Photolysis at 12.3% Efficiency via Perovskite Photovoltaics and Earth-abundant Catalysts. *Science* **2014**, *345*, 1593–1596.
- (5) Seitz, L. C.; Dickens, C. F.; Nishio, K.; Hikita, Y.; Montoya, J.; Doyle, A.; Kirk, C.; Vojvodic, A.; Hwang, H. Y.; Nørskov, J. K.; et al. A Highly Active and Stable IrOx/SrIrO₃ Catalyst for the Oxygen Evolution Reaction. *Science* **2016**, *353*, 1011–1014.
- (6) Danilovic, N.; Subbaraman, R.; Chang, K. C.; Chang, S. H.; Kang, Y.; Snyder, J.; Paulikas, A. P.; Strmcnik, D.; Kim, Y. T.; Myers, D.; et al. Using Surface Segregation to Design Stable Ru-Ir Oxides for the Oxygen Evolution Reaction in Acidic Environments. *Angew. Chem., Int. Ed.* **2014**, *53*, 14016–14021.
- (7) Huang, J.; Han, J.; Wang, R.; Zhang, Y.; Wang, X.; Zhang, X.; Zhang, Z.; Zhang, Y.; Song, B.; Jin, S. Improving Electrocatalysts for Oxygen Evolution Using Ni₃Fe_{3-x}O₄/Ni Hybrid Nanostructures Formed by Solvothermal Synthesis. *ACS Energy Lett.* **2018**, *3*, 1698–1707.
- (8) Wei, C.; Feng, Z.; Scherer, G. G.; Barber, J.; Shao-Horn, Y.; Xu, Z. J. Cations in Octahedral Sites: A Descriptor for Oxygen Electrocatalysis on Transition-Metal Spinel. *Adv. Mater.* **2017**, *29*, 1606800.
- (9) Yang, Y.; Dang, L.; Shearer, M. J.; Sheng, H.; Li, W.; Chen, J.; Xiao, P.; Zhang, Y.; Hamers, R. J.; Jin, S. Highly Active Trimetallic NiFeCr Layered Double Hydroxide Electrocatalysts for Oxygen Evolution Reaction. *Adv. Energy Mater.* **2018**, *8*, 1703189.
- (10) Qian, L.; Lu, Z.; Xu, T.; Wu, X.; Tian, Y.; Li, Y.; Huo, Z.; Sun, X.; Duan, X. Ternary Layered Double Hydroxides as High-Performance Bifunctional Materials for Oxygen Electrocatalysis. *Adv. Energy Mater.* **2015**, *5*, 1500245.
- (11) Feng, J. X.; Ye, S. H.; Xu, H.; Tong, Y. X.; Li, G. R. Design and Synthesis of FeOOH/CeO₂ Heterolayered Nanotube Electrocatalysts for the Oxygen Evolution Reaction. *Adv. Mater.* **2016**, *28*, 4698–4703.
- (12) Dionigi, F.; Strasser, P. NiFe-Based (Oxy)hydroxide Catalysts for Oxygen Evolution Reaction in Non-Acidic Electrolytes. *Adv. Energy Mater.* **2016**, *6*, 1600621.
- (13) Tang, D.; Liu, J.; Wu, X.; Liu, R.; Han, X.; Han, Y.; Huang, H.; Liu, Y.; Kang, Z. Carbon Quantum Dot/NiFe Layered Double-hydroxide Composite as a Highly Efficient Electrocatalyst for Water Oxidation. *ACS Appl. Mater. Interfaces* **2014**, *6*, 7918–7925.
- (14) Liang, H.; Meng, F.; Cabán-Acevedo, A. M.; Li, L.; Forticaux, A.; Xiu, L.; Wang, Z.; Jin, S. Hydrothermal Continuous Flow Synthesis and Exfoliation of NiCo Layered Double Hydroxide Nanosheets for Enhanced Oxygen Evolution Catalysis. *Nano Lett.* **2015**, *15*, 1421–1427.
- (15) Wu, W.; Zhang, S.; Ren, F.; Xiao, X.; Zhou, J.; Jiang, C. Controlled Synthesis of Magnetic Iron Oxides@SnO₂ Quasi-Hollow Core-Shell Heterostructures: Formation Mechanism, and Enhanced Photocatalytic Activity. *Nanoscale* **2011**, *3*, 4676–4684.
- (16) Wang, W. N.; An, W. J.; Ramalingam, B.; Mukherjee, S.; Niedzwiedzki, D. M.; Gangopadhyay, S.; Biswas, P. Size and Structure Matter: Enhanced CO₂ Photoreduction Efficiency by Size-Resolved Ultrafine Pt Nanoparticles on TiO₂ Single Crystals. *J. Am. Chem. Soc.* **2012**, *134*, 11276–11281.
- (17) Shim, J. H.; Lee, Y.; Kang, M.; Lee, J.; Baik, J. M.; Lee, Y.; Lee, C.; Kim, M. H. Hierarchically Driven IrO₂ Nanowire Electrocatalysts for Direct Sensing of Biomolecules. *Anal. Chem.* **2012**, *84*, 3827–3832.
- (18) Liu, Y.; Kang, Z. H.; Chen, Z. H.; Shafiq, I.; Zapien, J. A.; Bello, I.; Zhang, W. J.; Lee, S. T. Synthesis, Characterization, and Photocatalytic Application of Different ZnO Nanostructures in Array Configurations. *Cryst. Growth Des.* **2009**, *9*, 3222–3227.
- (19) Li, C.; Hong, G.; Wang, P.; Yu, D.; Qi, L. Wet Chemical Approaches to Patterned Arrays of Well-Aligned ZnO Nanopillars Assisted by Monolayer Colloidal Crystals. *Chem. Mater.* **2009**, *21*, 891–897.
- (20) Evans, D. G.; Duan, X. Preparation of Layered Double Hydroxides and Their Applications as Additives in Polymers, as Precursors to Magnetic Materials and in Biology and Medicine. *Chem. Commun.* **2006**, *37*, 485–496.
- (21) Dang, L. N.; Liang, H. F.; Zhuo, J. Q.; Lamb, B. K.; Sheng, H. Y.; Yang, Y.; Jin, S. Direct Synthesis and Anion Exchange of Noncarbonate-Intercalated NiFe-Layered Double Hydroxides and the Influence on Electrocatalysis. *Chem. Mater.* **2018**, *30*, 4321–4330.
- (22) Liu, W. J.; Dang, L.; Xu, Z.; Yu, H. Q.; Jin, S.; Huber, G. W. Electrochemical Oxidation of 5-Hydroxymethylfurfural with NiFe Layered Double Hydroxide (LDH) Nanosheet Catalysts. *ACS Catal.* **2018**, *8*, 5533–5541.
- (23) Abellán, G.; Coronado, E.; Martigastaldo, C.; Pinillaciencuegos, E.; Ribera, A. Hexagonal Nanosheets from The Exfoliation of Ni²⁺-Fe³⁺ LDHs: a Route towards Layered Multifunctional Materials. *J. Mater. Chem.* **2010**, *20*, 7451–7455.
- (24) Caravaggio, G. A.; Detellier, C.; Wronski, Z. Synthesis, Stability and Electrochemical Properties of NiAl and NiV Layered Double Hydroxides. *J. Mater. Chem.* **2001**, *11*, 912–921.
- (25) Liu, W.; Liu, H.; Dang, L.; Zhang, H.; Wu, X.; Yang, B.; Li, Z.; Zhang, X.; Lei, L.; Jin, S. Amorphous Cobalt-Iron Hydroxide Nanosheet Electrocatalyst for Efficient Electrochemical and Photoelectrochemical Oxygen Evolution. *Adv. Funct. Mater.* **2017**, *27*, 1603904.
- (26) Zheng, X.; Zhang, B.; De Luna, P.; Liang, Y.; Comin, R.; Voznyy, O.; Han, L.; García de Arquer, F. P.; Liu, M.; Dinh, C. T.; et al. Theory-Driven Design of High-Valence Metal Sites for Water Oxidation Confirmed Using In Situ Soft X-Ray Absorption. *Nat. Chem.* **2017**, *10*, 149–154.
- (27) Smith, R. D.; Prevot, M. S.; Fagan, R. D.; Zhang, Z.; Sedach, P. A.; Siu, M. K.; Trudel, S.; Berlinguette, C. P. Photochemical Route for Accessing Amorphous Metal Oxide Materials for Water Oxidation Catalysis. *Science* **2013**, *340*, 60–63.
- (28) Stevens, M.; Trang, C. D. M.; Enman, L. J.; Deng, J.; Boettcher, S. W. Reactive Fe-Sites in Ni/Fe (Oxy)Hydroxide Are Responsible for Exceptional Oxygen Electrocatalysis Activity. *J. Am. Chem. Soc.* **2017**, *139*, 11361–11364.
- (29) Mccrory, C. C. L.; Jung, S.; Ferrer, I. M.; Chatman, S. M.; Peters, J. C.; Jaramillo, T. F. Benchmarking Hydrogen Evolving Reaction and Oxygen Evolving Reaction Electrocatalysts for Solar Water Splitting Devices. *J. Am. Chem. Soc.* **2015**, *137*, 4347–4357.
- (30) Landon, J.; Demeter, E.; Inoglu, N.; Keturakis, C.; Wachs, I. E.; Vasić, R.; Frenkel, A. I.; Kitchin, J. R. Spectroscopic Characterization of Mixed Fe-Ni Oxide Electrocatalysts for the Oxygen Evolution Reaction in Alkaline Electrolytes. *ACS Catal.* **2012**, *2*, 1793–1801.
- (31) Kim, T. W.; Choi, K. S. Nanoporous BiVO₄ Photoanodes with Dual-Layer Oxygen Evolution Catalysts for Solar Water Splitting. *Science* **2014**, *343*, 990–994.
- (32) Gong, M.; Li, Y.; Wang, H.; Liang, Y.; Wu, J. Z.; Zhou, J.; Wang, J.; Regier, T.; Wei, F.; Dai, H. An Advanced Ni-Fe Layered Double Hydroxide Electrocatalyst for Water Oxidation. *J. Am. Chem. Soc.* **2013**, *135*, 8452–8455.

- (33) Louie, M. W.; Bell, A. T. An Investigation of Thin-Film Ni-Fe Oxide Catalysts for the Electrochemical Evolution of Oxygen. *J. Am. Chem. Soc.* **2013**, *135*, 12329–12337.
- (34) Smith, R. D.; Fagan, R. D.; Trudel, S.; Berlinguette, C. P. Water Oxidation Catalysis: Electrocatalytic Response to Metal Stoichiometry in Amorphous Metal Oxide Films Containing Iron, Cobalt, and Nickel. *J. Am. Chem. Soc.* **2013**, *135*, 11580–11586.
- (35) Smith, R. D.; Prévot, M. S.; Fagan, R. D.; Zhang, Z.; Sedach, P. A.; Siu, M. K.; Trudel, S.; Berlinguette, C. P. Photochemical Route for Accessing Amorphous Metal Oxide Materials for Water Oxidation Catalysis. *Science* **2013**, *340*, 60–63.
- (36) Trotochaud, L.; Ranney, J. K.; Williams, K. N.; Boettcher, S. W. Solution-Cast Metal Oxide Thin Film Electrocatalysts for Oxygen Evolution. *J. Am. Chem. Soc.* **2012**, *134*, 17253–17261.
- (37) Merrill, M. D.; Dougherty, R. C. Metal Oxide Catalysts for the Evolution of O₂ from H₂O. *J. Phys. Chem. C* **2008**, *112*, 3655–3666.
- (38) Lu, Z.; Xu, W.; Zhu, W.; Yang, Q.; Lei, X.; Liu, J.; Li, Y.; Sun, X.; Duan, X. Three-Dimensional NiFe Layered Double Hydroxide Film for High-Efficiency Oxygen Evolution Reaction. *Chem. Commun.* **2014**, *50*, 6479–6482.
- (39) Compton, O. C.; Nguyen, S. T. Graphene oxide, Highly Reduced Graphene Oxide, and Graphene: Versatile Building Blocks for Carbon-based Materials. *Small* **2010**, *6*, 711–723.
- (40) Zhang, Y.; Zhang, N.; Tang, Z.-R.; Xu, Y.-J. Graphene Transforms Wide Band Gap ZnS to a Visible Light Photocatalyst. The New Role of Graphene as a Macromolecular Photosensitizer. *ACS Nano* **2012**, *6*, 9777–9789.
- (41) Huang, X.; Yin, Z.; Wu, S.; Qi, X.; He, Q.; Zhang, Q.; Yan, Q.; Boey, F.; Zhang, H. Graphene-Based Materials: Synthesis, Characterization, Properties, and Applications. *Small* **2011**, *7*, 1876–1902.
- (42) Wang, H.; Xiang, X.; Li, F. Facile Synthesis and Novel Electrocatalytic Performance of Nanostructured Ni-Al Layered Double Hydroxide/Carbon Nanotube Composites. *J. Mater. Chem.* **2010**, *20*, 3944–3952.
- (43) An, X.; Shin, D.; Ocon, J. D.; Lee, J. K.; Son, Y. I.; Lee, J. Electrocatalytic Oxygen Evolution Reaction at a FeNi Composite on a Carbon Nanofiber Matrix in Alkaline Media. *Chin. J. Catal.* **2014**, *35*, 891–895.
- (44) Wang, Z.; Zeng, S.; Liu, W.; Wang, X. W.; Li, Q.; Zhao, Z.; Geng, F. Coupling Molecularly Ultrathin Sheets of NiFe-Layered Double Hydroxide on NiCo₂O₄ Nanowire Arrays for Highly Efficient Overall Water Splitting Activity. *ACS Appl. Mater. Interfaces* **2017**, *9*, 1488–1495.
- (45) Dong, L.; Chu, Y.; Sun, W. Controllable Synthesis of Nickel Hydroxide and Porous Nickel Oxide Nanostructures with Different morphologies. *Chem. - Eur. J.* **2008**, *14*, 5064–5072.
- (46) Liu, P. F.; Yang, S.; Zhang, B.; Yang, H. G. Defect-Rich Ultrathin Cobalt-Iron Layered Double Hydroxide for Electrochemical Overall Water Splitting. *ACS Appl. Mater. Interfaces* **2016**, *8*, 34474–34481.
- (47) Xu, H.; Wang, W.; Zhu, W. Sonochemical Synthesis of Crystalline CuS Nanoplates via an in Situ Template Route. *Mater. Lett.* **2006**, *60*, 2203–2206.
- (48) Abellán, G.; Coronado, E.; Martí-Gastaldo, C.; Ribera, A.; Otero, T. F. Magnetic Nanocomposites Formed by FeNi₃ Nanoparticles Embedded in Graphene. Application as Supercapacitors. *Part. Part. Syst. Char.* **2013**, *30*, 853–863.
- (49) Stevens, M. B.; Enman, L. J.; Batchellor, A. S.; Cosby, M. R.; Vise, A. E.; Trang, C. D. M.; Boettcher, S. W. Measurement Techniques for the Study of Thin Film Heterogeneous Water Oxidation Electrocatalysts. *Chem. Mater.* **2017**, *29*, 120–140.
- (50) Shinagawa, T.; Garcia-Esparza, A. T.; Takahabe, K. Insight on Tafel slopes from a Microkinetic Analysis of Aqueous Electrocatalysis for Energy Conversion. *Sci. Rep.* **2015**, *5*, 13801.
- (51) Wang, T.; Liu, L.; Zhu, Z.; Papakonstantinou, P.; Hu, J.; Liu, H.; Li, M. Enhanced Electrocatalytic Activity for Hydrogen Evolution Reaction from Self-assembled Monodispersed Molybdenum Sulfide Nanoparticles on an Au Electrode. *Energy Environ. Sci.* **2013**, *6*, 625–633.
- (52) Jin, H.; Wang, J.; Su, D.; Wei, Z.; Pang, Z.; Wang, Y. In Situ Cobalt-Cobalt Oxide/N-Doped Carbon Hybrids As Superior Bifunctional Electrocatalysts for Hydrogen and Oxygen Evolution. *J. Am. Chem. Soc.* **2015**, *137*, 2688–2694.
- (53) Han, T. A.; Tu, J. P.; Wu, J. B.; Li, Y.; Yuan, Y. F. Electrochemical Properties of Biphasic Ni(OH)₂ Electrodes for Secondary Rechargeable Ni/MH Batteries. *J. Electrochem. Soc.* **2006**, *153*, A738–A742.
- (54) Kiani, M. A.; Mousavi, M. F.; Ghasemi, S. Size Effect Investigation on Battery Performance: Comparison between Micro- and Nano-Particles of β-Ni(OH)₂ as Nickel Battery Cathode Material. *J. Power Sources* **2010**, *195*, 5794–5800.
- (55) Wei, H.; Lv, Y.; Han, L.; Tu, B.; Zhao, D. Facile Synthesis of Transparent Mesostructured Composites and Corresponding Crack-free Mesoporous Carbon/Silica Monoliths. *Chem. Mater.* **2011**, *23*, 2353–2360.
- (56) Friebe, D.; Louie, M. W.; Bajdich, M.; Sanwald, K. E.; Cai, Y.; Wise, A. M.; Cheng, M.; Sokaras, D.; Weng, T.; Alonsomori, R.; et al. Identification of Highly Active Fe Sites in (Ni,Fe)OOH for Electrocatalytic Water Splitting. *J. Am. Chem. Soc.* **2015**, *137*, 1305–1313.
- (57) Feng, Y.; Qiu, T. Preparation, Characterization and Microwave Absorbing Properties of FeNi Alloy Prepared by Gas Atomization Method. *J. Alloys Compd.* **2012**, *513*, 455–459.
- (58) Xiao, T.; Yang, C.; Lu, Y.; Zeng, F. One-pot Hydrothermal Synthesis of Rod-Like FeOOH/Reduced Graphene Oxide Composites for Supercapacitor. *J. Mater. Sci.: Mater. Electron.* **2014**, *25*, 3364–3374.
- (59) Zhang, X.; Liu, Y.; Dong, S.; Ye, Z.; Wei, Y. Low-Temperature Synthesized Nanocomposites with Amorphous FeOOH on Ti₃C₂X for Supercapacitors. *J. Alloys Compd.* **2018**, *744*, 507–519.
- (60) Tang, W.; Henkelman, G. Charge Redistribution in Core-Shell Nanoparticles to Promote Oxygen Reduction. *J. Chem. Phys.* **2009**, *130*, 194504.
- (61) Hammer, B.; Noerskov, J. K. Theoretical Surface Science and Catalysis-Calculations and Concepts. *Adv. Catal.* **2000**, *45*, 71–129.
- (62) Li, Y. F.; Selloni, A. Mechanism and Activity of Water Oxidation on Selected Surfaces of Pure and Fe-Doped NiOx. *ACS Catal.* **2014**, *4*, 1148–1153.
- (63) Chen, J.; Selloni, A. Water Adsorption and Oxidation at the Co₃O₄ (110) Surface. *J. Phys. Chem. Lett.* **2012**, *3*, 2808–2814.
- (64) Axmann, P.; Glemser, O. Nickel Hydroxide as a Matrix for Unusual Valencies: the Electrochemical Behaviour of Metal(III)-Ion-Substituted Nickel Hydroxides of the Pyroaurite Type. *J. Alloys Compd.* **1997**, *246*, 232–241.
- (65) Demourgues-Guerlou, L.; Fournès, L.; Delmas, C. On the Iron Oxidation State in the Iron-Substituted γ Nickel Oxyhydroxides. *J. Solid State Chem.* **1995**, *114*, 6–14.
- (66) Trotochaud, L.; Young, S. L.; Ranney, J. K.; Boettcher, S. W. Nickel-Iron Oxyhydroxide Oxygen-Evolution Electrocatalysts: The Role of Intentional and Incidental Iron Incorporation. *J. Am. Chem. Soc.* **2014**, *136*, 6744–6753.